Temperature Dependence of Viscosity and Specific Conductivity of Fluoroborate-Based Ionic Liquids in Light of the Fractional Walden Rule and Angell's Fragility Concept†

Christian Schreiner, Sandra Zugmann, Robert Hartl, and Heiner J. Gores*

Institute for Physical and Theoretical Chemistry, University of Regensburg, D-93040 Regensburg, Germany

Temperature-dependent conductivity and viscosity data of over ten new fluoroborate-based ionic liquids (ILs) were measured in a temperature range spanning about 100 K. Data are presented and evaluated according to the fractional Walden rule and Angell's fragility concept. All ILs show excellent linear relationships for their Walden plots with similar slopes in the range from about 0.90 to about 0.94. It was found empirically that the slopes of the Walden plots reflect the ratio of the corresponding Arrhenius activation energies for the ILs' temperature-dependent viscosities and molar conductivities. Further analysis of viscosity data of ILs leads to the conclusion that all investigated ILs, including some more common ones, can be classified as highly fragile, very weak liquids, reaching even the limiting value estimated by Vilgis.

Introduction

In a previous publication, temperature-dependent conductivities and viscosities of four common ionic liquids (ILs), namely, 1-ethyl-3-methylimidazolium tetrafluoroborate ([EMIM][BF_4]), 1-butyl-3-methylimidazolium tetrafluoroborate ([BMIM][BF_4]), 1-ethyl-3-methylimidazolium bis(trifluoromethanesulfonyl)imide ([EMIM][NTf_2]), and 1-ethyl-3-methylimidazolium dicyanamide ([EMIM][DCA]), have already been presented, together with a brief discussion of the fractional Walden rule and Walden plot.[1] This paper aims to extend this work on a series of new fluoroborate-based ILs derived from the corresponding tetrafluoroborate salts.[2] In addition to that, viscosity data were analyzed in light of the fragility concept which could be utilized to categorize different types of glass-forming liquids in general.

Ionic liquids are molten salts with unique properties making them favorable for many industrial applications, such as liquid−liquid extraction, catalysis, and electrochemical processes.[3−7] The most attention is dedicated to room-temperature ionic liquids (RTIL) which might replace traditional organic solvents for application in solar cells, fuel cells, double layer capacitors, and lithium ion batteries.[8−12] The highly temperature-dependent viscosity and conductivity of pure ILs is one of their key parameters. Especially at low temperatures, their viscosities are significantly higher than those for electrolyte solutions based on organic solvents, entailing lower conductivities.

Temperature Dependence of Ionic Liquids' Viscosity and Conductivity. Although we know that the viscosity η of liquids, which reflects the impulse transport, is not an activated process,[13] the Arrhenius equation is still used a lot to describe the viscosity's temperature dependence

$$\eta = \eta_0 \exp\left(\frac{E_a}{RT}\right) \tag{1}$$

η_0 is the limiting viscosity, E_a the activation energy, R the universal gas constant, and T the temperature. Because of the commonly found indirect proportionality between the viscosity and another transport property, the specific conductivity κ, the Arrhenius equation is also often applied to κ

$$\kappa = \kappa_0 \exp\left(\frac{-E'_a}{RT}\right) \tag{2}$$

Due to the deviation from a strictly linear Arrhenius-type relationship (eqs 1 and 2) and the physical background just mentioned, it is much better to fit $\eta - T$ and $\kappa - T$ data pairs by the empirically found Vogel−Fulcher−Tamman (VFT) eqs 3 and 4.[14−17]

$$\eta = \eta_0 \exp\left(\frac{B}{T - T_0}\right) = \eta_0 \exp\left(\frac{DT_0}{T - T_0}\right) \tag{3}$$

$$\kappa = \kappa_0 \exp\left(\frac{-B'}{T - T'_0}\right) \tag{4}$$

where B is a fittting parameter, and T_0 is the ideal glass transition temperature. The parameter D used in the alternative form of the VFT eq 3 can be used to describe the "strength" of a liquid (see below). The VFT equation usually allows an exceptionally precise data fitting and interpolation in a given temperature range and a fairly good extrapolation beyond these limits too.

Fractional Walden Rule. The empirically discovered relation between the limiting molar conductivity Λ_m^0 of an electrolyte and the pure solvent's viscosity η, which is known as the Walden rule,[18] states that the product of both properties is constant for infinitely diluted electrolytes, as given in eq 5

$$\Lambda_m^0 \eta = C = \text{constant} \tag{5}$$

† Part of the "Sir John S. Rowlinson Festschrift".

* Corresponding author. Tel.: +49(0)941/9434746. Fax: +49(0)941/9434532. E-mail address: heiner.gores@chemie.uni-regensburg.de.

10.1021/je1005505
Published on Web 07/20/2010

To account for deviations from this ideal case, an additional exponent α could be introduced to give the fractional Walden rule, eq 6.[19−22] Taking the logarithm of this equation results in a linear relationship (eq 7) that allows us to obtain the exponent α as the slope and log(*C*′) as the graph's intercept.

$$\Lambda_m{}^0 \eta^\alpha = C' = \text{constant} \tag{6}$$

$$\log \Lambda_m{}^0 = \log(C') + \alpha \log \eta^{-1} \tag{7}$$

Up to now, there have been no systematic studies concerning the exponent α. We have to go back in the literature to the pioneering book of Robinson and Stokes, where related work of R. H. Stokes was reported: In a series of $\eta(T)$ and $\kappa(T)$ measurements at aqueous electrolyte solutions with added solutes, such as sucrose, mannitol, and glycerol, it was found that α is roughly a linear function of the molar volume of the nonelectrolyte for a given electrolyte. For a given nonelectrolyte, α increases with the molar volume of an nonelectrolyte ion, reaching unity for very large ions.

Surprisingly, the fractional Walden rule holds true not only for many dilute and concentrated electrolyte solutions but also for temperature-dependent data of pure molten salts, i.e., ILs. Here, viscosity and conductivity data points of neat ILs measured at the same temperatures could be paired and correlated in the Walden plot and by eqs 5 to 7 in the same manner. Instead of the electrolyte solution's limiting molar conductivity $\Lambda_m{}^0$, the pure IL's molar conductivity Λ_m is used for this purpose. Λ_m is calculated by eq 8 from the IL's specific conductivity κ and molar volume V_m which is in turn obtained from the IL's density ρ and molar mass M.

$$\Lambda_m = \kappa V_m = \kappa \frac{M}{\rho} \tag{8}$$

Ionic Liquids' Fragility. The fragility concept, first introduced by Angell,[23−25] can be utilized to categorize liquids for their temperature-dependent viscosity. The fragility m is defined as the limiting slope in a plot of $\log(\eta)$ vs T_G/T at the glass transition temperature T_G. It is a measure for the viscosity's temperature dependence at the glass transition temperature. The larger the value of m, the higher the fragility and the stronger the viscosity change for a temperature increment at T_G. The following short subsection summarizes the pathway to the desired simple relationship between m and D.

$$m = \frac{d(\log \eta)}{d(T_G/T)}^{T=T_G} \tag{9}$$

Applying this definition to the VFT equation with the strength parameter $D = B/T_0$ yields

$$m = \frac{DT_0}{\ln 10} \cdot \frac{T_G}{(T_G - T_0)^2} \tag{10}$$

The kinetic glass transition temperature is usually defined as the temperature at which the viscosity exceeds 10^{15} mPa·s.[25] As the viscosity changes over many orders of magnitude within a very small temperature range, at the glass transition temperature, its actual value used for this approach is not that crucial for the final results, so to be consistent with the literature, $\eta(T_G) \equiv 10^{15}$ mPa·s has been used as well. Another common observation is that the limiting viscosity η_0 is about 10^{-1} mPa·s for very "infinitely" high temperatures. This leads to the conclusion that the viscosity typically spans about 16 orders of magnitude between $T \rightarrow \infty$ and T_G.

For strict Arrhenius behavior, the fragility has its minimum m_{min} obtained by applying eq 9 to the Arrhenius eq 1[24]

$$m_{min} = \log\left(\frac{\eta(T_G)}{\eta_0}\right) \approx 16 \tag{11}$$

On the other hand, this and the fragility definition applied to the VFT equation yields

$$m_{min} = \frac{DT_0}{\ln 10} \frac{1}{(T_G - T_0)} \tag{12}$$

and after some rearrangements

$$\frac{T_G}{T_0} = 1 + \frac{D}{m_{min} \ln 10} \tag{13}$$

and

$$m = m_{min} + \frac{\ln 10}{D} m_{min}^2 \tag{14}$$

This finally shows the indirect proportionality between the fragility m and the strength parameter D; with $m_{min} \approx 16$, it is simply[26]

$$m \approx 16 + \frac{590}{D} \tag{15}$$

This is a rather useful relation between m and D as Vilgis[27] derived a model relation between D and the average coordination number z_0 of molecules in the liquid phase (i.e., the average number of neighbors) and its variability Δz.

$$D = \frac{1}{4}\left(\frac{z_0}{\Delta z}\right)^2 \tag{16}$$

Strong liquids (small m, large D) have a very low variability Δz of the average coordination number z_0. Prototypes for this class are molten network-forming glasses such as SiO_2, GeO_2, and B_2O_3, for which typical values of z_0 are around 3 to 5. They are dominated by strong direct intermolecular interactions and a high resistance against structural change upon heating. Weak or fragile liquids on the other hand have weaker, nondirectional intermolecular interactions with a much higher variability Δz. Molecules form a nonorganized dense packing in the liquid with high fluctuations. This leads to a higher susceptibility toward structural change upon temperature change, hence a high fragility. For the lower limit of D, $z_0 \approx 14$ and $\Delta z \approx 4$ have been estimated, leading to $D_{min} \approx 3.2$; this corresponds to an upper limit for the fragility of $m_{max} \approx 200$. Typical examples for highly fragile liquids are melts of organic glass formers such as *o*-terphenyl, propylene carbonate, and some polymers.[24]

Experimental Section

Materials. The ionic liquids 1-ethyl-3-methylimidazolium difluoromono(oxalato)borate ([EMIM][[BF_2Ox], 1-butyl-3-methylimidazolium difluoromono(oxalato)borate ([BMIM][BF_2Ox]), 1-ethyl-3-methylimidazolium difluoromono(malonato)borate ([EMIM][BF_2Ma]), 1-butyl-3-methylimidazolium difluoromono(malonato)borate ([BMIM][BF_2Ma]), 1-ethyl-3-methylimidazolium difluorobis(acetato)borate ([EMIM][$BF_2(Ac)_2$]), 1-butyl-3-methylimidazolium difluorobis(acetato)borate ([BMIM][$BF_2(Ac)_2$]), tetraethylammonium difluorobis(acetato)borate ([TEA][$BF_2(Ac)_2$]), 1-ethyl-3-methylimidazolium difluorobis(trifluoroacetato)borate ([EMIM][$BF_2(TFA)_2$]), 1-butyl-3-methylimidazolium difluorobis(trifluoroacetato)borate ([BMIM][$BF_2(TFA)_2$]), tetraethylammonium difluorobis(trifluoroacetato)borate ([TEA][$BF_2(TFA)_2$]), and tetraethylammonium difluoromono(oxalato)borate ([TEA][BF_2Ox]) were synthesized according to previously published procedures in a chloride-free manner from the corresponding tetrafluoroborate salts and trimethylsilyl compounds.[2] All ILs had a water content (weight fraction) of less than 10^{-4} as determined by Karl Fischer titration (Mettler, Karl Fischer Titrator DL18). IL storage and handling was done in an argon-filled glovebox (MBraun, type MB150BG, $x(O_2)$ and $x(H_2O)$ both $< 10^{-6}$).

Conductivity Measurements. Conductivity measurements were carried out with an in-house built symmetrical Wheatstone-bridge, with Wagner earth, resistance decade, and sine generator as already described earlier.[28] The calibration of the conductivity cells as well as the thermostat setup which allows a temperature stability of ± 2 mK are described elsewhere.[29,30] Temperatures were monitored using an ASL F-250 MkII thermometer (Automatic Systems Laboratories). On the basis of the calibration data of individual measuring cells, the estimated uncertainty of the measured specific conductivities is in the range of (0.2 to 0.4) %.

Viscosity Measurements. Viscosities were measured with a modified automated AVS/G Ubbelohde capillary viscometer (Schott) as described in ref 31, using two micro-Ubbelohde capillaries (Schott Instruments, type 537 20/II and III) placed in a Dewar flask that was connected to the high-precision thermostat with a circulation pump, giving a temperature control of ± 3 mK. In-house built modifications allowed keeping samples under dry nitrogen throughout the whole measurement procedure to prevent any water uptake. The manufacturer's original capillary calibrations were confirmed successfully and improved with a certified viscosity standard oil (50 BW, ZMK-Analytik, relative uncertainty 0.32 %) at temperatures of (293.15, 296.15, 298.15, 303.15, and 313.15) K with a flow time reproducibility between individual runs of better than ± 0.05 %. On the basis of the temperature and calibration standard's accuracy and measurement reproducibility, the estimated uncertainty of presented viscosity data which has been averaged over multiple runs is about 0.5 %.

Density Measurements. Ionic liquids' densities were determined with a precision densitometer DMA 60/DMA 602 from Anton Paar in a temperature range from (298.15 to 333.15) K. Temperature control (better than ± 0.02 K) was maintained by a RK 8 KP thermostat from LAUDA and controlled by a temperature sensor close to the measuring cell. Measured densities were fitted accurately with a second-order polynomial to inter- and extrapolate ILs' densities as required for data evaluation over the whole temperature range. The estimated uncertainty of the measured densities is below 0.01 %.

Thermal Analysis. Ionic liquids' glass transition temperatures required for the fragility analysis have already been published in ref 2, together with other thermal analysis results determined by standard DSC and TGA measurements.

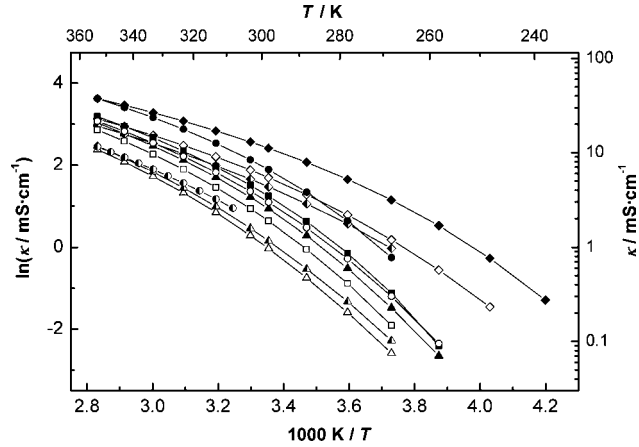

Figure 1. Arrhenius plot of ILs' temperature-dependent conductivity data for filled circle, [EMIM][BF_2Ox]; open circle, [BMIM][BF_2Ox]; semifilled circle, [TEA][BF_2Ox]; filled square, [EMIM][BF_2Ma]; open square, [BMIM][BF_2Ma]; filled triangle, [EMIM][$BF_2(Ac)_2$]; open triangle, [BMIM][$BF_2(Ac)_2$]; semifilled triangle, [TEA][$BF_2(Ac)_2$]; filled diamond, [EMIM][$BF_2(TFA)_2$]; open diamond, [BMIM][$BF_2(TFA)_2$]; and semifilled diamond, [TEA][$BF_2(TFA)_2$].

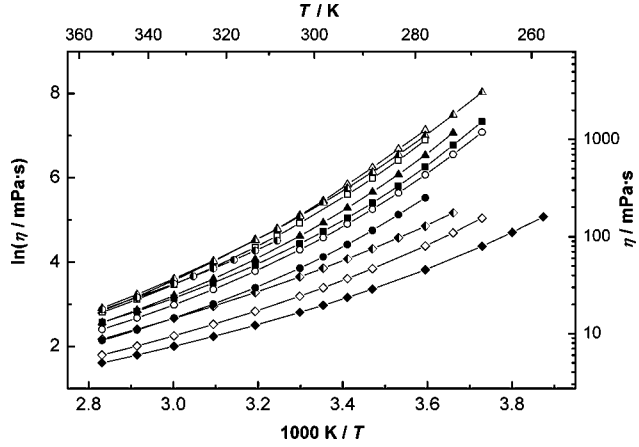

Figure 2. Arrhenius plot of ILs' temperature-dependent viscosity data for filled circle, [EMIM][BF_2Ox]; open circle, [BMIM][BF_2Ox]; semifilled circle, [TEA][BF_2Ox]; filled square, [EMIM][BF_2Ma]; open square, [BMIM][BF_2Ma]; filled triangle, [EMIM][$BF_2(Ac)_2$]; open triangle, [BMIM][$BF_2(Ac)_2$]; semifilled triangle, [TEA][$BF_2(Ac)_2$]; filled diamond, [EMIM][$BF_2(TFA)_2$]; open diamond, [BMIM][$BF_2(TFA)_2$]; semifilled diamond, [TEA][$BF_2(TFA)_2$].

Results and Discussion

Detailed measurement data of density, conductivity, and viscosity are given in the Supporting Information. Figure 1 shows the Arrhenius plot for the ILs' temperature-dependent specific conductivities κ, and Figure 2 shows the Arrhenius plot for their viscosities η, respectively. Table 1 holds the obtained VFT fit parameters for all ILs.

Compared to [EMIM][BF_4] and [BMIM][BF_4], similar ILs with [BF_2Ox]$^-$, [$BF_2(Ac)_2$]$^-$, and [$BF_2(Ac)_2$]$^-$ anions instead of the [BF_4]$^-$ possess higher viscosities, with [BMIM][$BF_2(Ac)_2$] being the most viscous IL. On the other hand, [$BF_2(TFA)_2$]$^-$ anions lead to a significant reduction of IL viscosities, with [EMIM][$BF_2(TFA)_2$]$^-$ being the least viscous IL. This clearly demonstrates the impact of fluorination on charge delocalization which affects the coordination ability of the [$BF_2(TFA)_2$]$^-$ anion. With regard to its size and volume, shape and surface charge

Table 1. Fitting Parameters for VFT Equations 3 and 4, Describing ILs' Viscosity and Conductivity, Respectively[a]

	η_0	B	T_0	κ_0	B'	T_0'
ionic liquid	10^{-2} mPa·s	K	K	mS·cm^{-1}	K	K
[EMIM][BF_2Ox]	18.52 ± 1.89	602.34 ± 18.53	194.60 ± 1.37	751.81 ± 6.62	451.39 ± 2.18	202.75 ± 0.29
[BMIM][BF_2Ox]	8.25 ± 1.38	814.61 ± 29.95	183.10 ± 1.62	754.25 ± 24.67	547.49 ± 8.51	199.13 ± 0.99
[TEA][BF_2Ox]	18.36 ± 1.30	781.18 ± 19.21	182.30 ± 1.67	696.33 ± 55.17	690.88 ± 23.93	184.70 ± 2.56
[EMIM][BF_2Ma]	12.85 ± 3.44	728.78 ± 43.55	190.48 ± 2.38	741.36 ± 6.79	521.19 ± 2.34	201.03 ± 0.28
[BMIM][BF_2Ma]	11.32 ± 0.46	819.38 ± 7.73	187.77 ± 0.44	973.12 ± 34.34	621.56 ± 9.39	198.57 ± 0.98
[EMIM][$BF_2(Ac)_2$]	13.19 ± 1.44	743.55 ± 18.75	191.34 ± 1.06	971.59 ± 23.46	600.71 ± 6.44	197.08 ± 0.70
[BMIM][$BF_2(Ac)_2$]	4.61 ± 1.64	1027.67 ± 78.95	177.79 ± 4.24	1014.77 ± 70.10	722.24 ± 19.21	194.27 ± 1.80
[TEA][$BF_2(Ac)_2$]	5.52 ± 0.34	1033.88 ± 12.85	173.67 ± 0.65	1108.62 ± 56.49	743.70 ± 14.57	189.62 ± 1.37
[EMIM][$BF_2(TFA)_2$]	23.53 ± 0.41	550.49 ± 3.35	173.67 ± 0.29	573.50 ± 4.91	487.81 ± 2.47	174.34 ± 0.35
[BMIM][$BF_2(TFA)_2$]	16.00 ± 0.14	653.75 ± 1.80	173.04 ± 0.14	531.24 ± 6.94	552.95 ± 3.79	177.44 ± 0.48
[TEA][$BF_2(TFA)_2$]	14.86 ± 1.41	777.65 ± 23.02	163.21 ± 1.78	625.37 ± 10.10	642.12 ± 5.03	168.93 ± 0.59

[a] As the parameters in this and the following tables may also be used for data interpolation, the number of significant digits exceeds that specified by the estimated uncertainty.

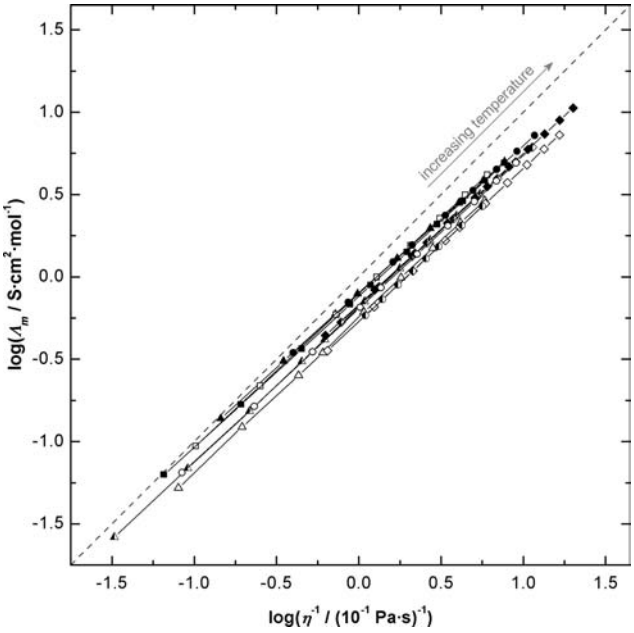

Figure 3. Walden plot for filled circle, [EMIM][BF_2Ox]; open circle, [BMIM][BF_2Ox]; semifilled circle, [TEA][BF_2Ox]; filled square, [EMIM][BF_2Ma]; open square, [BMIM][BF_2Ma]; filled triangle, [EMIM][$BF_2(Ac)_2$]; open triangle, [BMIM][$BF_2(Ac)_2$]; semifilled triangle, [TEA][$BF_2(Ac)_2$]; filled diamond, [EMIM][$BF_2(TFA)_2$]; open diamond, [BMIM][$BF_2(TFA)_2$]; semifilled diamond, [TEA][$BF_2(TFA)_2$]. The dashed straight line has a slope of 1.

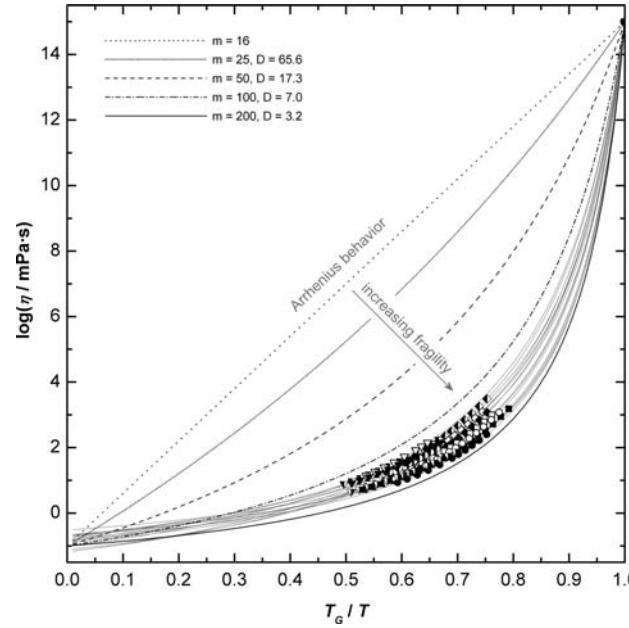

Figure 4. Fragility plot for filled circle, [EMIM][BF_2Ox]; open circle, [BMIM][BF_2Ox]; semifilled circle, [TEA][BF_2Ox]; filled square, [EMIM][BF_2Ma]; open square, [BMIM][BF_2Ma]; filled triangle, [EMIM][$BF_2(Ac)_2$]; open triangle, [BMIM][$BF_2(Ac)_2$]; semifilled triangle, [TEA][$BF_2(Ac)_2$]; filled diamond, [EMIM][$BF_2(TFA)_2$]; open diamond, [BMIM][$BF_2(TFA)_2$]; semifilled diamond, [TEA][$BF_2(TFA)_2$]. This plot also shows filled inverted triangle, [EMIM][BF_4]; open inverted triangle, [BMIM][BF_4]; right-hand side semifilled inverted triangle, [EMIM][DCA]; and left-hand side semifilled inverted triangle, [EMIM][NTf_2]. Data taken from ref 1. Lines depict theoretical curves for fragilities $m = 16$ (dotted), $m = 25$ (short dashed), $m = 50$ (dashed), $m = 100$ (dashed dotted), and $m = 200$ (solid).

density, and distribution, this anion is pretty similar to the well-known, weakly coordinating bis(trifluoromethanesulfonyl)imide anion which leads to low viscous, hydrophobic ILs as well.[1,32]

The Walden plot (Figure 3) for all ILs shows excellent linear relationships according to the fractional Walden rule. Linear fits give the slope which is the exponent α of the fractional Walden rule (eq 6). The slope α and the intercept log(C') of all ILs are pretty comparable (Table 2). This means that there are no major differences for example in ion pairing or ion screening between all those ILs. This could be expected due to the similarities in chemical structures. As pointed out in ref 1, it is not that easy to draw simple conclusions between the values of α and log(C') and other IL properties.

However, the Walden plot directly correlates the ILs' temperature-dependent (molar) conductivities and viscosities. A slope/exponent of $\alpha = 1$ would mean that the molar conductivity and the viscosity would have a perfectly inverse temperature dependence so that one would decrease to the same extent as the other increases. By utilizing the Arrhenius equation, this would lead to the very same activation energy for both the viscosity and (molar) conductivity. Any deviation from $\alpha = 1$ would resemble a difference between the activation energies for the ILs' viscosities, $E_a^{\eta}(T)$, and for their specific conductivities, $E_a^{\kappa}(T)$, or more accurately for their molar conductivities, $E_a^{\Lambda}(T)$. To check the hypothesis that α from the Walden plot is the same as the ratio between the viscosity and conductivity activation energies, all curves in the Arrhenius plots were fitted to a cubic polynomial. All fit parameters and the Arrhenius plot for the molar conductivities are given in the Supporting Information. As the Arrhenius plots have a slight curvature over the measured range, the activation energies are not temperature independent, but for each individual temperature they could be obtained as the tangents to those Arrhenius plot curves. This was achieved by differentiation of all obtained fit equations and calculating the activation energies within the fitted data range. Then, the ratios of $E_a^{\kappa}(T)$ to $E_a^{\eta}(T)$ and $E_a^{\Lambda}(T)$ to $E_a^{\eta}(T)$ were calculated and averaged

Table 2. Linear Fitting Parameters for Fractional Walden Plots According to Equation 7[a]

ionic liquid	α	log(C'/S·cm^2·mol^{-1})
[EMIM][BF_2Ox]	0.89786 ± 1.5·10^{-3}	−0.09974 ± 9.8·10^{-4}
[BMIM][BF_2Ox]	0.92761 ± 1.0·10^{-3}	−0.19395 ± 6.6·10^{-4}
[TEA][BF_2Ox]	0.93352 ± 1.7·10^{-3}	−0.27188 ± 7.7·10^{-4}
[EMIM][BF_2Ma]	0.91583 ± 5.8·10^{-4}	−0.11891 ± 3.7·10^{-4}
[BMIM][BF_2Ma]	0.92986 ± 9.8·10^{-4}	−0.10437 ± 5.7·10^{-4}
[EMIM][BF_2(Ac)$_2$]	0.90412 ± 1.4·10^{-3}	−0.09960 ± 7.9·10^{-4}
[BMIM][BF_2(Ac)$_2$]	0.93911 ± 2.9·10^{-3}	−0.24987 ± 1.7·10^{-3}
[TEA][BF_2(Ac)$_2$]	0.93980 ± 1.5·10^{-3}	−0.18624 ± 1.1·10^{-3}
[EMIM][BF_2(TFA)$_2$]	0.91827 ± 3.0·10^{-4}	−0.16958 ± 2.6·10^{-4}
[BMIM][BF_2(TFA)$_2$]	0.92902 ± 6.4·10^{-4}	−0.27006 ± 5.0·10^{-4}
[TEA][BF_2(TFA)$_2$]	0.91305 ± 1.9·10^{-3}	−0.17283 ± 1.3·10^{-3}

[a] Standard deviations for all linear fits in the Walden plot were < 0.2 %, with $R^2 > 0.99999$.

over their ranges (see Table 3). It could be easily seen that $E_a^{\Lambda}(T)/E_a^{\eta}(T)$ perfectly matches α from the fractional Walden rule. In average, $E_a^{\Lambda}(T)/E_a^{\eta}(T)$ is just (0.22 ± 0.17) % lower than α for all ILs. The same trend is observed for the specific conductivity κ, but due to the additional change of the molar volume over the temperature range, the ratio $E_a^{\kappa}(T)/E_a^{\eta}(T)$ is (1.91 ± 0.34) % lower than α for all ILs.

Table 4 holds the results for the VFT fits and fragility analysis of all ILs, and Figure 4 shows the corresponding fragility plot. Fits differ a bit from the ones in Table 1 as $\eta(T_G) \equiv 10^{15}$ mPa·s at T_G as an additional data point has been included as described above. The strength parameter D for all ILs ranges between 3.1 and 5.8, and the average is 4.31 ± 0.83. This corresponds with fragility values m between 118.8 and 195.7, and the average is 154.6 ± 24.2. Hence, all ILs could be classified as extremely weak and fragile liquids, an interesting finding due to its implications for the liquid state interactions. Equation 13 allows an estimation for T_G/T_0, with $m_{min} \approx 16$ follows $T_G/T_0 \approx 1 + 0.0271D$. The ratios of T_G from DSC measurements and T_0 from the VFT fit match this relation very well, and the average ratio is $T_G/T_0 \approx 1.12 \pm 0.02$. The difference between the ideal glass transition temperature T_0 which has also been identified as the Kauzmann temperature[33,34] and the measured glass transition temperatures T_G^{DSC} is rather small, in average only about (20.6 ± 3.5) K, while a common rule of thumbs says that this difference is roughly about ≈50 K. The high fragility seems to be connected to the observed extensive supercooling tendency and low glass transition temperatures for ILs.

Conclusions

Temperature-dependent viscosity, conductivity, and density data of a series of fluoroborate-based ionic liquids were presented and analyzed by the fragility concept and the fractional

Table 3. Comparison of α from the Walden Plot with the Ratios of the Activation Energies for the ILs' Viscosity, $E_a^{\eta}(T)$, Specific Conductivity, $E_a^{\kappa}(T)$, and Molar Conductivity, $E_a^{\Lambda}(T)$[a]

ionic liquid	$E_a^{\kappa}(T)/E_a^{\eta}(T)$	$E_a^{\Lambda}(T)/E_a^{\eta}(T)$	α
[EMIM][BF_4]	0.8878 ± 7.5·10^{-3}	0.9030 ± 3.3·10^{-3}	0.90419 ± 7.7·10^{-4}
[BMIM][BF_4]	0.9135 ± 1.4·10^{-2}	0.9286 ± 5.6·10^{-3}	0.93024 ± 8.4·10^{-4}
[EMIM][DCA]	0.9301 ± 1.0·10^{-2}	0.9469 ± 7.2·10^{-3}	0.94946 ± 7.5·10^{-4}
[EMIM][NTf_2]	0.8880 ± 1.8·10^{-2}	0.9044 ± 7.6·10^{-3}	0.90588 ± 1.2·10^{-3}
[EMIM][BF_2Ox]	0.8822 ± 1.4·10^{-2}	0.8982 ± 6.1·10^{-3}	0.89786 ± 1.5·10^{-3}
[BMIM][BF_2Ox]	0.9117 ± 8.8·10^{-3}	0.9252 ± 5.1·10^{-3}	0.92761 ± 1.0·10^{-3}
[TEA][BF_2Ox]	0.9152 ± 7.9·10^{-3}	0.9330 ± 5.5·10^{-3}	0.93352 ± 1.7·10^{-3}
[EMIM][BF_2Ma]	0.9052 ± 7.3·10^{-3}	0.9138 ± 4.6·10^{-3}	0.91583 ± 5.8·10^{-4}
[BMIM][BF_2Ma]	0.9159 ± 1.0·10^{-2}	0.9280 ± 6.0·10^{-3}	0.92986 ± 9.8·10^{-4}
[EMIM][BF_2(Ac)$_2$]	0.8862 ± 1.5·10^{-2}	0.9027 ± 4.4·10^{-3}	0.90412 ± 1.4·10^{-3}
[BMIM][BF_2(Ac)$_2$]	0.9202 ± 1.5·10^{-2}	0.9337 ± 9.9·10^{-3}	0.93911 ± 2.9·10^{-3}
[TEA][BF_2(Ac)$_2$]	0.9238 ± 1.4·10^{-2}	0.9345 ± 1.3·10^{-2}	0.93980 ± 1.5·10^{-3}
[EMIM][BF_2(TFA)$_2$]	0.8976 ± 1.4·10^{-2}	0.9178 ± 2.1·10^{-3}	0.91827 ± 3.0·10^{-4}
[BMIM][BF_2(TFA)$_2$]	0.9067 ± 1.3·10^{-2}	0.9284 ± 4.2·10^{-3}	0.92902 ± 6.4·10^{-4}
[TEA][BF_2(TFA)$_2$]	0.8892 ± 1.6·10^{-2}	0.9093 ± 1.0·10^{-2}	0.91305 ± 1.9·10^{-3}

[a] Data for [EMIM][BF_4], [BMIM][BF_4], [EMIM][DCA], and [EMIM][NTf_2] were taken from ref 1 and evaluated accordingly.

Table 4. VFT Fitting Parameters for All Plots with $\eta(T_G) \equiv 10^{15}$ mPa·s as an Additional Data Point, At the Glass Transition Temperature T_G^{DSC} Determined by DSC[a]

		B	T_0	T_G^{DSC}			$T_G - T_0$	
ionic liquid	log(η_0/10^{-2} mPa·s)	K	K	K	D	m	K	T_G/T_0
[EMIM][BF_4]	−0.69078 ± 0.00265	713.17 ± 0.97	160.46 ± 0.02	180.2 ± 0.6	4.44 ± 0.01	143.23 ± 0.21	19.7	1.123
[BMIM][BF_4]	−1.01443 ± 0.00548	941.44 ± 2.25	163.87 ± 0.05	189.4 ± 0.2	5.75 ± 0.02	118.81 ± 0.32	25.5	1.156
[EMIM][DCA]	−0.51933 ± 0.00548	512.71 ± 1.76	165.45 ± 0.04	179.8 ± 1.0	3.10 ± 0.01	195.73 ± 0.72	14.3	1.086
[EMIM][NTf_2]	−0.72987 ± 0.00457	740.20 ± 1.72	154.86 ± 0.04	175.3[b]	4.78 ± 0.01	134.88 ± 0.35	(20.4)	1.132
[EMIM][BF_2Ox]	−0.76302 ± 0.01023	625.56 ± 3.03	192.01 ± 0.07	209.3 ± 1.3	3.26 ± 0.02	191.27 ± 1.00	17.2	1.090
[BMIM][BF_2Ox]	−0.90628 ± 0.00660	738.22 ± 1.92	187.59 ± 0.04	207.8 ± 0.3	3.94 ± 0.01	163.11 ± 0.46	20.2	1.108
[TEA][BF_2Ox]	−0.73001 ± 0.00314	776.63 ± 1.18	182.76 ± 0.03	204.2[b]	4.25 ± 0.01	149.83 ± 0.25	(21.4)	1.117
[EMIM][BF_2Ma]	−0.69905 ± 0.01008	660.99 ± 2.80	194.06 ± 0.06	212.4 ± 0.8	3.41 ± 0.02	182.22 ± 0.83	18.3	1.094
[BMIM][BF_2Ma]	−0.85705 ± 0.00297	776.27 ± 0.93	190.64 ± 0.02	211.9 ± 1.0	4.07 ± 0.01	158.05 ± 0.21	21.3	1.112
[EMIM][BF_2(Ac)$_2$]	−1.12086 ± 0.01803	873.84 ± 5.90	182.26 ± 0.13	205.8 ± 0.6	4.79 ± 0.04	140.94 ± 1.05	23.5	1.129
[BMIM][BF_2(Ac)$_2$]	−1.17727 ± 0.0125	951.95 ± 4.28	181.59 ± 0.09	207.2 ± 0.3	5.24 ± 0.03	131.09 ± 0.65	25.6	1.141
[TEA][BF_2(Ac)$_2$]	−1.18524 ± 0.00672	1001.93 ± 2.33	175.06 ± 0.05	202.0 ± 0.1	5.72 ± 0.01	121.53 ± 0.32	26.9	1.154
[EMIM][BF_2(TFA)$_2$]	−0.66001 ± 0.00173	567.21 ± 0.54	172.02 ± 0.01	187.8 ± 0.5	3.30 ± 0.01	186.92 ± 0.19	15.7	1.091
[BMIM][BF_2(TFA)$_2$]	−0.83791 ± 0.0028	679.18 ± 0.95	170.63 ± 0.02	189.3 ± 0.1	3.98 ± 0.01	161.01 ± 0.24	18.6	1.109
[TEA][BF_2(TFA)$_2$]	−0.80599 ± 0.00473	760.07 ± 1.71	165.02 ± 0.04	185.9 ± 0.5	4.61 ± 0.01	140.75 ± 0.35	20.9	1.127

[a] T_G^{DSC} is the average T_G from the cooling and the heating run, and the given error is the deviation of the average from the individual values. Data and VFT Fits for [EMIM][BF_4], [BMIM][BF_4], [EMIM][DCA], and [EMIM][NTf_2] were taken from ref 1 and given here for comparison. D is the IL's strength which corresponds inversely to the fragility m which has been obtained from the fit; m has been calculated from D by eq 14. [b] No glass transition could been observed by DSC measuring as the sample crystallized during the cooling run before reaching T_G. Therefore, its value has been estimated by the $T_G/T_{fus} \approx 2/3$ rule. The chosen value has only a minor impact on D and m because T_0 shifts with a change in T_G accordingly.

Walden rule. All ILs show pretty comparable behavior in terms of their very high fragility and their fractional Walden rule exponent. Although the ILs do not strictly obey Arrhenius behavior, it was found that the fractional Walden rule's exponent α, which is the slope of the linear Walden plots, equals the ratio of the temperature-dependent activation energies for viscosity and (molar) conductivity.

Acknowledgment

Thanks to Prof. Alexander Apelblat, Professor Emeritus, Ben Gurion University of the Negev, Chemical Engineering Department, POB 653, Beer Sheva, 84105 Israel, for valuable comments concerning the fractional Walden rule. This paper is dedicated to Sir John S. Rowlinson for his contributions to the advancement of the knowledge of liquids that has been a continuing inspiration for us.

Supporting Information Available:

Measured temperature-dependent conductivity, viscosity, and density data for given ionic liquids and additional data fits. This material is available free of charge via the Internet at http://pubs.acs.org.

Literature Cited

(1) Schreiner, C.; Zugmann, S.; Hartl, H.; Gores, H. J. Fractional Walden Rule for Ionic Liquids: Examples from Recent Measurements and a Critique of the So-Called Ideal KCl Line for the Walden Plot. *J. Chem. Eng. Data* **2010**, *55*, 1784–1788.
(2) Schreiner, C.; Amereller, M.; Gores, H. J. Chloride-Free Method to Synthesise New Ionic Liquids with Mixed Borate Anions. *Chem.—Eur. J.* **2009**, *15*, 2270–2272.
(3) Welton, T. Room-Temperature Ionic Liquids. Solvents for Synthesis and Catalysis. *Chem. Rev.* **1999**, *99*, 2071–2083.
(4) Huddleston, J. G.; Willauer, H. D.; Swatloski, R. P.; Visser, A. E.; Rogers, R. D. Physical Room temperature ionic liquids as novel media for 'clean' liquid-liquid extraction. *Chem. Commun.* **1998**, 1765–1766.
(5) Wasserscheid, P.; Keim, W. Ionische Fluessigkeiten - innovative Loesungsmittel. *Nachr. Chem.* **2001**, 12–16.
(6) Galinski, M.; Lewandowski, A.; Stepniak, I. Ionic liquids as electrolytes. *Electrochim. Acta* **2006**, *51*, 5567–5580.
(7) Borgel, V.; Markevich, E.; Aurbach, D.; Semrau, G.; Schmidt, M. On the application of ionic liquids for rechargeable Li batteries: High voltage systems. *J. Power Sources* **2009**, *189*, 331–336.
(8) Wachter, P.; Schreiner, C.; Zistler, M.; Gerhard, D.; Wasserscheid, P.; Gores, H. J. A microelectrode study of triiodide diffusion coefficients in mixtures of room temperature ionic liquids, useful for dye-sensitised solar cells. *Microchim. Acta* **2008**, *160*, 125–133.
(9) Zistler, M.; Wachter, P.; Wasserscheid, P.; Gerhard, D.; Hinsch, A.; Sastrawan, R.; Gores, H. J. Comparison of electrochemical methods for triiodide diffusion coefficient measurements and observation of non-Stokesian diffusion behaviour in binary mixtures of two ionic liquids. *Electrochim. Acta* **2006**, *52*, 161–169.
(10) Herzig, T.; Schreiner, C.; Bruglachner, H.; Jordan, S.; Schmidt, M.; Gores, H. J. Temperature and Concentration Dependence of Conductivities of Some New Semi-chelatoborates in Acetonitrile and Comparison with other Borates. *J. Chem. Eng. Data* **2008**, *53*, 434–438.
(11) De Souza, R. F.; Padilha, J. C.; Gonçalves, R. S.; Dupont, J. Room temperature dialkylimidazolium ionic liquid-based fuel cells. *Electrochem. Commun.* **2003**, *5*, 728–731.
(12) Moosbauer, D.; Zugmann, S.; Amereller, M.; Gores, H. J. Effect of Ionic Liquids as Additives on Lithium Electrolytes Conductivity, Electrochemical Stability, and Aluminum Corrosion. *J. Chem. Eng. Data* **2010**, *55*, 1794–1798.
(13) Alder, B. J.; Einwohner, T. Free-Path Distribution for Hard Spheres. *J. Chem. Phys.* **1965**, *43*, 3399–3400.
(14) Vogel, H. Das Temperaturabhängigkeitsgesetz der Viskosität von Flüssigkeiten. *Phys. Zeit.* **1921**, *22*, 645–646.
(15) Fulcher, G. S. Analysis of Recent Measurements of the Viscosity of Glasses. *J. Am. Ceram. Soc.* **1952**, *8*, 339–355.
(16) Tammann, G.; Hesse, W. Die Abhängigkeit der Viscosität von der Temperatur bei unterkühlten Flüssigkeiten. *Z. Anorg. Allg. Chem.* **1926**, *156*, 245–257.
(17) Scherer, G. W. Editorial Comments on a Paper by Gordon S. Fulcher. *J. Am. Ceram. Soc.* **1992**, *75*, 1060–1062.
(18) Walden, P. Über organische Lösungs- und Ionisierungsmittel. III. Teil: Innere Reibung und deren Zusammenhang mit dem Leitvermögen. *Z. Phys. Chem.* **1906**, *55*, 207–246.
(19) Robinson, R. A.; Stokes, R. H. *Electrolyte Solutions*; Butterworths: London, 1968; pp 307−309.
(20) Xu, W.; Cooper, E. I.; Angell, C. A. Ionic Liquids: Ion Mobilities, Glass Temperatures, and Fragilities. *J. Phys. Chem. B* **2003**, *107*, 6170–6178.
(21) Pugsley, F. A.; Wetmore, F. E. W. Molten Salts: Viscosity of Silver Nitrate. *Can. J. Chem.* **1954**, *32*, 839–841.
(22) Frenkel, J. *Kinetic theorv of liquids*; The Clarendon Press: Oxford, 1946.
(23) Angell, C. A. Relaxation in liquids, polymers and plastic crystals - strong/fragile patterns and problems. *J. Non-Cryst. Solids* **1991**, *131−133*, 13–31.
(24) Böhmer, R.; Ngai, K. L.; Angell, C. A.; Plazek, D. J. Nonexponential relaxations in strong and fragile glass formers. *J. Chem. Phys.* **1993**, *99*, 4201–4209.
(25) Angell, C. A. Formation of Glasses from Liquids and Biopolymers. *Science* **1995**, *267*, 1924–1935.
(26) Hodge, I. M. Strong and fragile liquids - a brief critique. *J. Non-Cryst. Solids* **1991**, *202*, 164–172.
(27) Vilgis, T. A. Strong and fragile glasses - A powerful classification and its consequences. *Phys. Rev. B* **1993**, *47*, 2882–2885.
(28) Barthel, J.; Wachter, R.; Gores, H. J. *Modern Aspects of Electrochemistry*; Bockris, J. O'M., Conway, B. E., Eds; Plenum: New York, 1979; Vol. 13, pp 1−79.
(29) Barthel, J.; Feuerlein, F.; Neueder, R.; Wachter, R. Calibration of Conductance Cells at Various Temperatures. *J. Solution Chem.* **1980**, *9*, 209–219.
(30) Wachter, R.; Barthel, J. Studies on the temperature dependence of properties of electrolyte solutions. Part II. Conductivity determination over a large temperature range. *Ber. Bunsenges. Phys. Chem.* **1979**, *83*, 634–642.
(31) Kindler, M. Transporteigenschaften nichtwässriger Elektrolytlösungen für Hochenergiebatterien mit Lithium als Anode. Dissertation, University Regensburg, 1985.
(32) Schreiner, C. Synthese und Charakterisierung neuer Ionischer Flüssigkeiten auf der Basis gemischter Fluoroborat-Anionen. Dissertation, University Regensburg, 2009.
(33) Adam, G.; Gibbs, J. H. On the Temperature Dependence of Cooperative Relaxation Properties in Glass-Forming Liquids. *J. Chem. Phys.* **1965**, *43*, 139–146.
(34) Kauzmann, W. The Nature of the Glassy State and the Behavior of Liquids at Low Temperatures. *Chem. Rev.* **1948**, *43*, 219–256.

Received for review May 25, 2010. Accepted July 6, 2010. Financial support from the German Research Foundation (DFG), contract number 544243, Project Initiative PAK 177 "Funktionsmaterialien und Materialanalytik zu Lithium-Hochleistungsbatterien" and by the DFG priority program SPP 1191 "Ionic Liquids" is gratefully acknowledged.

JE1005505